Multi-class maximum likelihood expectation-maximization list-mode image reconstruction

Mehdi Latif, Jérôme Idier, Thomas Carlier, Simon Stute

Multi-class maximum likelihood expectation-maximization list-mode image reconstruction: an application to three-gamma imaging

Mehdi Latif[1,2], Jérôme Idier[1], Thomas Carlier[2], and Simon Stute[2]

[1]Nantes Université, École Centrale Nantes, LS2N, CNRS, UMR 6004, F-44000 Nantes, France
[2]Nantes Université, CHU Nantes, CRCI2NA, F-44000 Nantes, France

Abstract Our contribution focuses at improving the image reconstruction process for specific Compton imaging systems able to detect multiple classes of events, in the field of nuclear imaging. For each existing prototype of such systems, one or several processing methods have already been proposed to retrieve the activity map. Most of them get their inspiration from maximum likelihood expectation-maximization (MLEM), but none of them actually compute the MLEM solution. Some exploit the fully detected events only (e.g. in three-gamma imaging, the simultaneous detection of a pair of annihilation photons and of a third photon), and other combine several classes of detected events in a suboptimal way. In this paper, we first introduce a general framework for the reconstruction of a single activity map from multi-class events, and we provide the suited list-mode MLEM update equation. We then consider the case of XEMIS2, a preclinical prototype of a Compton telescope for three-gamma imaging, for which four distinct classes of partial detections coexist with the full detection class. As a preliminary step towards effective multi-class reconstruction, we generate a sensitivity map for the five classes using a dedicated Monte Carlo simulator.

1 Introduction

In nuclear imaging, some scanner prototypes based on Compton imaging allow the detection of different types of events. For instance,

- The MACACO camera [1] is a Compton telescope with three layers of plane detectors having different energy resolutions. Photon (or gamma) interactions in different combinations of layers lead to events with different spatial resolution properties.
- The WGI preclinical prototype [2] has a full-ring geometry with a scatterer detector close to the scanned subject and an absorber further away. In addition to Compton imaging, WGI performs positron emission tomography (PET) imaging by detecting annihilation photons in coincidence. With radio-isotopes emitting nearly simultaneously a positron and a (third) gamma, 3-gamma (3γ) imaging can be performed [3]. The emission point can be localized near the intersection of the Compton cone-of-response (COR) of the third gamma and the PET line-of-response (LOR) of the annihilation photons.
- The XEMIS2 preclinical prototype [4] is a Compton telescope using liquid xenon as a single continuous detection medium. It has been specifically designed for 3γ imaging.

All scanners described above detect distinct types of events during a single acquisition. To avoid the widespread term *type*, we call them *classes* of events hereafter.

In terms of image reconstruction, the WGI prototype separately considers Compton or PET image reconstructions [2]. With 3γ, a single back-projection is performed [3]. For XEMIS2, a method has been proposed to transform 3γ data into TOF PET data in order to use conventional PET reconstruction methods [5]. Only 3γ data were used while single or double γ events were discarded. For MACACO, all event classes were considered together in the reconstruction process. An extension of the MLEM algorithm was proposed lacking a theoretical derivation, where the update term is the sum of contributions from each event class and weighted by the sum of the sensitivities of each class [6].

Here, we first introduce a theoretical framework for the reconstruction of a single activity map from multi-class events. In particular, we derive a proper list-mode MLEM algorithm suited to the multi-class case. In a second stage, we consider 3γ imaging based on XEMIS2 as a specific case. As a preliminary step towards effective multi-class reconstruction, we generate a sensitivity map for each class using a dedicated Monte Carlo simulator.

2 Derivation of the multi-class list-mode MLEM

In what follows, $\boldsymbol{\lambda} := \{\lambda_j\}_{j\in[\![1,J]\!]}$ denotes a voxelized density of events, where each λ_j represents the expected number of emitted events from the jth voxel. As mentioned earlier, we consider a multi-class data approach, where the available information about $\boldsymbol{\lambda}$ arises from several distinct datasets.

2.1 Multi-class data

Let $\boldsymbol{y} := \{\boldsymbol{y}_n\}_{n\in[\![1,N]\!]}$ be the set of N collected data. It is composed of $K \in \mathbb{N}^*$ disjoint classes of physically independent events. A class refers to a specific type of event that can be detected and identified. We assume that each observed event can be attributed to one class, so that the set $\boldsymbol{y}$ can be expressed as the union of K independent classes:

$$\boldsymbol{y} := \bigcup_{k=1}^{K} \{\boldsymbol{y}_n^k\}_{n\in[\![1,N^k]\!]}, \qquad N = \sum_{k=1}^{K} N^k, \tag{1}$$

where each $\boldsymbol{y}_n^k \in \mathbb{R}^{d^k}$ is a measurement vector containing photon interaction coordinates and deposited energies for the nth event.

2.2 Multi-class likelihood

We assume that within each class k, the events $\left\{\boldsymbol{y}_n^k\right\}_{n\in[\![1,N^k]\!]}$ are independent and identically distributed (iid) according to the probability density function of sampling $\boldsymbol{y}^k$ from any point of the $\boldsymbol{\lambda}$ distribution:

$$\boldsymbol{y}_n^k \sim p^k\left(\boldsymbol{y}^k|\boldsymbol{\lambda}\right) \quad \forall k \in [\![1,K]\!]. \tag{2}$$

The log-likelihood function then reads:

$$l(\boldsymbol{\lambda}|\boldsymbol{y}) := \sum_{k=1}^{K}\sum_{n=1}^{N^k} \ln p^k\left(\boldsymbol{y}_n^k|\boldsymbol{\lambda}\right) = \sum_{k=1}^{K} l^k\left(\boldsymbol{\lambda}|\boldsymbol{y}^k\right) \tag{3}$$

where $l^k(\boldsymbol{\lambda}|\boldsymbol{y}^k)$ denotes the log-likelihood of the kth class. Under standard Poisson assumptions, we can decompose $l^k\left(\boldsymbol{\lambda}|\boldsymbol{y}^k\right)$ as

$$l^k\left(\boldsymbol{\lambda}|\boldsymbol{y}^k\right) := \sum_{n=1}^{N^k} \ln\left(\sum_{j=1}^{J} a_{nj}^k \lambda_j\right) - N^k \ln\left(\sum_{j=1}^{J} \lambda_j s_j^k\right), \tag{4}$$

where $a_{nj}^k := A_j^k\left(\boldsymbol{y}_n^k\right)$ defines an element of the system matrix specific to class k and voxel j, expressed as a continuous function of the nth measurement vector, and s_j^k denotes the sensitivity of voxel j for class k:

$$s_j^k := \int_{v\in\Omega^k} A_j^k(v)\,\mathrm{d}v \quad \forall j \in [\![1,J]\!],\ k \in [\![1,K]\!], \tag{5}$$

where Ω^k denotes the continuous detection domain related to the kth class.

2.3 Multi-class list-mode MLEM

To perform the estimation of $\boldsymbol{\lambda}$, we must extend the list-mode MLEM algorithm [7, 8] to simultaneously account for the K classes. The result is the following update equation:

$$\widehat{\lambda}_j^{(t+1)} := \widehat{\lambda}_j^{(t)} \times \frac{1}{\sum_k s_j^k} \sum_{k=1}^{K}\sum_{n=1}^{N^k} a_{nj}^k \frac{1}{\sum_{j'} a_{nj'}^k \widehat{\lambda}_{j'}^{(t)} + \varepsilon_n^k}, \tag{6}$$

where ε_n^k can be used to modelled random and scatter detections for each class. For a complete derivation of (6), we first need to express the log-likelihood of the complete dataset, along the same lines as in [7]. In the multi-class framework, a specific property is that the latter is a sum over the K classes. The update equation (6) is then obtained from (3) within the model of the EM algorithm [9] and allowing the decomposition of the auxiliary function $Q(\boldsymbol{\lambda}|\boldsymbol{\lambda}^{(t)})$ into a sum of lower bound approximation on the likelihood for each class:

$$Q^k\left(\boldsymbol{\lambda}|\boldsymbol{\lambda}^{(t)}\right) := \mathbb{E}_{\boldsymbol{z}^k|\boldsymbol{y}^k,\boldsymbol{\lambda}^{(t)}}\left(\ln p^k(\boldsymbol{y}^k,\boldsymbol{z}^k \mid \boldsymbol{\lambda})\right) \forall k \in [\![1,K]\!] \tag{7}$$

where $\boldsymbol{z}^k$ denotes the latent data vector.

3 Application to three-gamma imaging

3.1 XEMIS2 camera

The above results can be applied to XEMIS2, in the context of 3γ imaging. This imaging modality makes use of an isotope that quasi-simultaneously emits a positron (leading to the annihilation in two photons of 511 keV) and a so-called third photon. In our application, scandium-44 (^{44}Sc) is used where the third photon is isotropically emitted with an energy of 1157 keV. The XEMIS2 camera is a preclinical prototype based on a continuous cylindrical liquid xenon (LXe) detector [4]. The axial length of the active zone is 24 cm with an internal (resp. external) radius of 7 cm (resp. 19 cm). The design of the camera only allows to operate at low count rates resulting in low random rates. The energy resolution at 511 keV is 9% (FWHM) which would allowed to remove most of scattered photon using a tight energy window.

3.2 Classes of detections with XEMIS2

Based on the energy of the detected photons, $K = 5$ classes of events are possible:

- $1\gamma_{\mathrm{COR}}^{511}$ events correspond to the detection of a single annihilation photon. Its emission position belongs to a COR with a half-opening angle $\beta \in [0,\pi]$ given by the Compton scattering angle formula:

$$\beta := \operatorname{acos}\left(1 - \frac{m_e c^2 E_1}{E_0\,(E_0 - E_1)}\right) \tag{8}$$

  where $m_e c^2$ is the mass energy of an electron, E_0 is the total energy of the incident photon, i.e. $E_0 = 511$ keV for this class, and E_1 is the energy deposited in the detection medium during the scattering effect.

- $1\gamma_{\mathrm{COR}}^{1157}$ events correspond to the detection of the third photon. Akin to the former case, it is possible to define a COR using eq. (8) with $E_0 = 1157$ keV.

- $2\gamma_{\mathrm{LOR}}$ events correspond to the detection of both annihilation photons. As standard PET imaging, the source of annihilation belongs to a LOR.

- $2\gamma_{\mathrm{COR}}$ events correspond to the detection of a single annihilation photon and the third photon (combination of $1\gamma_{\mathrm{COR}}^{511}$ and $1\gamma_{\mathrm{COR}}^{1157}$). The origin of the decay belongs to the intersection of the two CORs.

- 3γ events correspond to the independent combination of a $2\gamma_{\mathrm{LOR}}$ event with a $1\gamma_{\mathrm{COR}}^{1157}$ one.

The imaging procedures currently available for XEMIS2 (*e.g.*, [5]) only exploit 3γ events. The other classes correspond to partial detections. Yet, they could bring additional information to the image reconstruction process, and thus lead to estimated activity maps $\widehat{\boldsymbol{\lambda}}$ of enhanced quality using a suited multi-class reconstruction algorithm such as eq. (6).

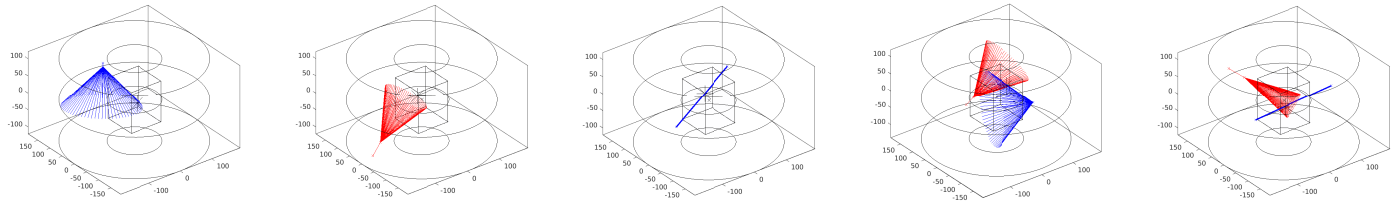

(a) $1\gamma^{511}_{\mathrm{COR}}$ (b) $1\gamma^{1157}_{\mathrm{COR}}$ (c) $2\gamma_{\mathrm{LOR}}$ (d) $2\gamma_{\mathrm{COR}}$ (e) 3γ

Figure 1: Examples of detection obtained with the Monte Carlo simulator dedicated to XEMIS2. The LXe continuous detection medium is represented by the hollow cylinder, and the studied image by the box in the center. Blue LORs and CORs are obtained from annihilation photon(s), and red CORs from the third photon.

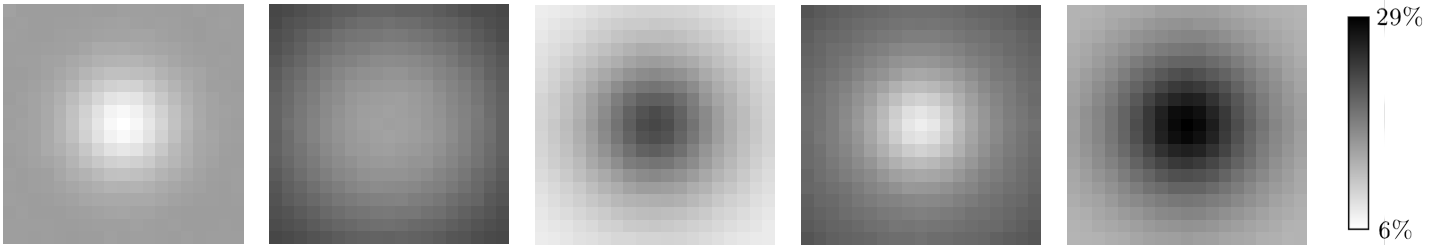

(a) $1\gamma^{511}_{\mathrm{COR}}$ (b) $1\gamma^{1157}_{\mathrm{COR}}$ (c) $2\gamma_{\mathrm{LOR}}$ (d) $2\gamma_{\mathrm{COR}}$ (e) 3γ

Figure 2: A cross-section of the sensitivity maps (%) for each class of event at $z = 0$.

3.3 Monte Carlo simulator

Multi-class image reconstruction can be first assessed through simulation. To this end, a Monte Carlo simulator was implemented to generate 3γ emissions and their detection in a continuous medium, according to the geometry of XEMIS2. It is based on a ray-tracing method, allowing us to simulate emissions from voxels within the field-ov-view (FOV) by randomly selecting three directional vectors to define the positron range, the trajectories of the annihilation photons along the LOR, and the third photon. Once a photon reaches the LXe zone, new random draws were performed to simulate the mean free path and the radiation-matter interactions that may occur, such as Compton scattering, Rayleigh scattering and photoelectric effect. Cross-section values were extracted from the XCOM database [10]. We neglect the Rayleigh effect since its normalized cross-section is strictly lower than 10% over the entire energy range of interest i.e. for energies lower than 1157 keV. The resulting code, named Pollux, is open-source and freely available at mlatif/tep3g-pollux. Fig. 1 presents examples of detection for each event class obtained with Pollux.

3.4 Sensitivity computation of XEMIS2

The mathematical expression of the voxelwise sensitivity (5) involves multi-integrals that cannot be evaluated analytically. We thus used Pollux to generate approximate maps of the sensitivity for an empty FOV. To this end, the whole FOV was discretized into $19 \times 19 \times 24$ voxels of $5 \times 5 \times 10\,\mathrm{mm}^3$. $M = 2 \times 10^5$ 3γ emission points were uniformly generated in each voxel and the event class was recorded for each emission.

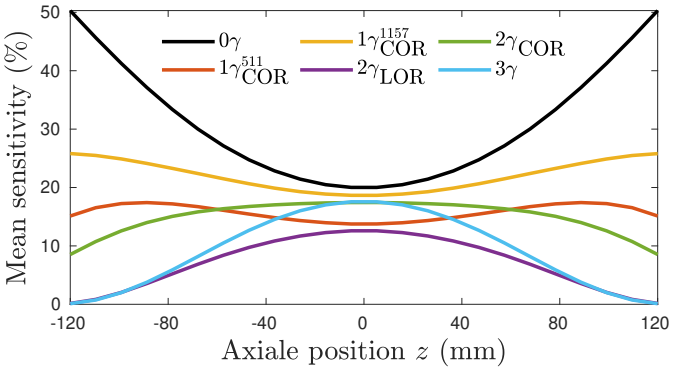

Figure 3: Mean sensitivity (%) along the axial direction for each class of event. The 0γ curve corresponds to the mean distribution of non-detected emissions.

Fig. 2 displays the sensitivity map obtained for each class for a transaxial cross-section at the center of the FOV, while Fig. 3 shows the same maps along the axial direction. The sensitivity distributions of the different classes are spatially heterogeneous, and tend to complement each other, which is an interesting observation in the perspective of multi-class reconstruction. For instance, the sensitivity maps of classes 3γ and $2\gamma_{\mathrm{LOR}}$ are maximal at the center of the FOV, while the trend is reversed for the sensitivity of $1\gamma^{511}_{\mathrm{COR}}$ and $1\gamma^{1157}_{\mathrm{COR}}$. Let us remark that non-detected events can be gathered in a sixth class 0γ, whose "sensitivity map" (as displayed in Fig. 3) can rather be understood as a non-sensitivity one.

Table 1 displays the distribution of detected events by class, which represent 69% of the emissions that led to the detection of at least one photon. We note that approximately 13% of the emissions lead to the detection of 3γ, which is small

compared to the partially detected events, totalizing almost 87% of all cases. Obviously, we expect the most informative events to be in the 3γ class, and the $2\gamma_{\text{LOR}}$ events to be more informative than the other events on CORs. However, 3γ and $2\gamma_{\text{LOR}}$ classes represent about a quarter of the detected events.

Class	$1\gamma^{511}_{\text{COR}}$	$1\gamma^{1157}_{\text{COR}}$	$2\gamma_{\text{LOR}}$	$2\gamma_{\text{COR}}$	3γ
% of detection	22.86	32.07	10.2	21.67	13.2

Table 1: Classification of detected events ($\approx 69\%$) for emissions uniformly distributed within the set voxels in the discretized FOV.

4 Discussion and perspectives

Our contribution focuses at designing an image reconstruction process for specific Compton imaging systems able to detect multiple classes of events, in the field of nuclear imaging.

First, we introduced a theoretical framework for the reconstruction of a single activity map from multi-class events, from which we deduced the suited list-mode MLEM update equation. The latter is potentially applicable to several existing prototypes of Compton imaging systems, such as MACACO, WGI, and XEMIS2. Let us also mention that the multi-class version of MLEM could be extended to cases where a regularization term is considered, as proposed in [11], for instance.

In a second part, we made a step further towards an application to XEMIS2, which is a preclinical prototype of a Compton telescope for 3γ imaging. In the XEMIS2 case, four distinct classes of partial detections coexist with the 3γ class. Using a dedicated Monte Carlo simulator, we determined a sensitivity map specific to each class, which is prerequisite to implement our multi-class version of MLEM. Besides, the obtained sensitivity maps clearly indicate that partial detections are far more frequent than perfect detections. Moreover, we noticed that some partial detection classes spatially complement the 3γ class. On the one hand, each partial detection is less informative than a full detection, but on the other hand, partial detections are more frequent. An interesting task will be to determine the amount of information brought by each class. This could be formally achieved by expressing the Fisher Information Matrix in the multi-class case, as an extension of the standard framework of [7]. We could then anticipate which classes are worth to be incorporated, despite the increased computational cost.

The next important step of our project will be the implementation of the proposed multi-class MLEM algorithm on the CASToR (Customizable and Advanced Software for Tomographic Reconstruction) platform [12]. Based on Pollux simulations, we are currently working at allowing continuous measurements and COR events within the CASToR framework. We also plan to implement a more realistic simulator using the GEANT4 toolkit [13].

Acknowledgments

The authors thank Nicolas Beaupère for valuable discussions about the XEMIS2 detector and events processing. This work has been partly funded by the NExT Junior Talent project TRAC through the French “Programme d’Investissement Avenir”.

References

[1] E. Muñoz, J. Barrio, A. Etxebeste, et al. “Performance evaluation of MACACO: a multilayer Compton camera”. *Phys. Med. Biol.* 62.18 (Aug. 2017), pp. 7321–7341. DOI: 10.1088/1361-6560/aa8070.

[2] H. Tashima, E. Yoshida, H. Wakizaka, et al. “3D Compton image reconstruction method for whole gamma imaging”. *Phys. Med. Biol.* 65.22 (Nov. 2020), p. 225038. DOI: 10.1088/1361-6560/abb92e.

[3] A. Mohammadi, H. Tashima, S. Takyu, et al. “Feasibility of triple gamma ray imaging of ^{10}C for range verification in ion therapy”. *Phys. Med. Biol.* 67.16 (Aug. 2022), p. 165001. DOI: 10.1088/1361-6560/ac826a.

[4] L. Gallego Manzano, J. Abaline, S. Acounis, et al. “XEMIS2: A liquid xenon detector for small animal medical imaging”. *NIM-A* 912 (Dec. 2018), pp. 329–332. DOI: 10.1016/j.nima.2017.12.022.

[5] D. Giovagnoli, A. Bousse, N. Beaupere, et al. “A Pseudo-TOF Image Reconstruction Approach for Three-Gamma Small Animal Imaging”. *IEEE Trans. Radiat. Plasma Med. Sci.* 5.6 (Nov. 2021), pp. 826–834. DOI: 10.1109/TRPMS.2020.3046409.

[6] J Roser, L Barrientos, J Bernabéu, et al. “Joint image reconstruction algorithm in Compton cameras”. *Phys. Med. Biol.* 67.15 (Aug. 2022), p. 155009. DOI: 10.1088/1361-6560/ac7b08.

[7] L. Parra and H. Barrett. “List-mode likelihood: EM algorithm and image quality estimation demonstrated on 2-D PET”. *IEEE Trans. Med. Imag.* 17.2 (Apr. 1998), pp. 228–235. DOI: 10.1109/42.700734.

[8] S. Wilderman, N. Clinthorne, J. Fessler, et al. “List-mode maximum likelihood reconstruction of Compton scatter camera images in nuclear medicine”. *1998 IEEE NSS/MIC*. Vol. 3. 1998, 1716–1720 vol.3. DOI: 10.1109/NSSMIC.1998.773871.

[9] A. P. Dempster, N. M. Laird, and D. B. Rubin. “Maximum Likelihood from Incomplete Data Via the *EM* Algorithm”. *J. R. Statist. Soc. B* 39.1 (Sept. 1977), pp. 1–22. DOI: 10.1111/j.2517-6161.1977.tb01600.x.

[10] “XCOM: Photon Cross Sections Database”. *NIST* (Sept. 2009).

[11] A. De Pierro. “A modified expectation maximization algorithm for penalized likelihood estimation in emission tomography”. *IEEE Trans. Med. Imag.* 14.1 (Mar. 1995), pp. 132–137. DOI: 10.1109/42.370409.

[12] T. Merlin, S. Stute, D. Benoit, et al. “CASToR: a generic data organization and processing code framework for multi-modal and multi-dimensional tomographic reconstruction”. *Phys. Med. Biol.* 63.18 (Sept. 2018), p. 185005. DOI: 10.1088/1361-6560/aadac1.

[13] S. Agostinelli, J. Allison, K. Amako, et al. “Geant4—a simulation toolkit”. *NIM-A* 506.3 (July 2003), pp. 250–303. DOI: 10.1016/S0168-9002(03)01368-8.